Core dependence of electron emission in slow collisions of highly charged ions (Ar^{16+},Kr^{16+},Xe^{16+}) with C_{60}

J. Bernard, R. Brédy, S. Martin, L. Chen, J. Désesquelles, and M. C. Buchet-Poulizac
Laboratoire de Spectrométrie Ionique et Moléculaire (UMR CNRS 5579), Université Lyon 1, Campus de la Doua, F-69622 Villeurbanne Cedex, France

(Received 25 February 2002; published 30 July 2002)

We present experimental results concerning an isocharge study of multielectronic capture and stabilization in slow collisions of Ar^{16+}, Xe^{16+}, Kr^{16+} with C_{60}. Partial multicapture cross sections σ_r^s are given for all observed channels. The core effect only has an effect when the number of transferred electrons is sufficiently high. In this case, the stabilization ratio has been found equal to 4.2, 3.6, and 2.9 for Ar^{16+}, Kr^{16+}, and Xe^{16+}, respectively. These measurements are qualitatively explained by fewer steps in the autoionization cascades for Xe than for Ar.

DOI: 10.1103/PhysRevA.66.013209 PACS number(s): 36.40.−c

I. INTRODUCTION

Collisions between slow highly charged ions (SHCI) and C_{60} started to be of great interest during the past decade [1,2] since high amounts of C_{60} were available to produce intense molecular target beams of C_{60} [3]. The interest comes from the fact that SHCI-C_{60} collisions generate multiexcited states on the projectile with many electrons in high-lying Rydberg states via multielectron capture from the C_{60}, while more internal shells are transitorily unoccupied. These so-called ''hollow atoms,'' observed before in SHCI-surface interactions, are very unstable versus autoionization processes and are responsible for the emission of a great number of electrons in the continuum. To help further discussions let us define now, accordingly to previous papers [4,5], r, the total number of active electrons that are transferred from the C_{60} to the projectile, n, the number of ejected electrons, and s, the number of stabilized electrons (electrons remaining on the projectile when all autoionization processes have occurred) and let us recall here the simple rule issued from the total charge conservation law: $r=n+s$. Since the first experiments of collisions between SHCI and C_{60}, concerning Ar^{8+} or later Xe^{q+}, for instance, several features were immediately noticed. First, the number of active electrons could exceed largely the initial charge of the projectile. This feature had never been observed before in SHCI-atom collisions. For instance, Martin *et al.* [6] reported the measurement of up to 80 active electrons for $s=13$ in Xe^{30+}-C_{60} collisions. Secondly, for Ar^{8+} a small enhancement of the cross section σ_s has been observed for $s=6$ and 7 [1]. This ''hump'' was later interpreted as due to collisions with impact parameters close or smaller than the C_{60} cage radius [4,6]. This assumption has been confirmed by measuring an energy loss of around 300 eV, comparable to the theoretical value of an Ar^{8+} colliding with a 3.2-Å-thick carbon foil. These collisions at impact parameters smaller than the C_{60} cage radius are referred as ''solidlike'' collisions in opposition to high impact parameter collisions that are qualified as ''atomlike'' collisions. It seemed reasonable then to define a transition regime, called ''surfacelike,'' with a rather blurry high impact parameter limit corresponding to the case when r approximately equals the projectile charge. Langereis *et al.* [7] have presented systematic measurements of cross sections for stabilizing s electrons in Ar^{q-}-C_{60} collisions with $q=4-18$. Their results show an overall increase of the σ^s with increasing projectile charges for $s=1$ and 2, more or less constant σ^s values for $s=4-6$ except for a deep fall of σ^5 and σ^6 occurring at the so-called ''high-q'' charge states ($q\geqslant 10$), which can be explained by the opening of the L shell.

Concerning theoretical aspects, it is largely admitted that the transfer of electrons from the C_{60} to the SHCI can be described by an overbarrier model assuming C_{60} as a conducting sphere and including image charge effects [2,8]. Thumm developed a postcollisional autoionization model that is relevant for atomlike collisions only. Martin *et al.* have extended the overbarrier model including a screening constant that allows the capture of a greater number of electrons. Though the image charge interaction has been neglected in the potential, the model fitted correctly the experimental total cross sections for Xe^{25+}-C_{60} with a screening constant of 0.4 [9]. In contrast, to our actual knowledge, no model has been proposed to account correctly for autoionizing processes in order to calculate partial σ_r^s cross sections. However, Palmeri *et al.* [10] have recently presented calculations of Auger rates for hollow atom configurations and deduced averaged lifetimes for a few atoms. For instance, for hollow xenon atoms with 30 electrons in the $n=20$ shell, the average lifetime is found to be 4.6×10^{-16} s.

In this paper, we present measurements of σ_r^s cross sections in collisions between the isocharge series of projectiles Ar^{16+}, Kr^{16+}, Xe^{16+}, and C_{60} targets. The partial cross section σ_r^s is associated with a collision channel corresponding to s electrons stabilized on the projectile from r active electrons. These experimental data provide information on the projectile atomic core structure dependence of the electron emission and stabilization in the three collision regimes (atomlike, surfacelike, and solidlike).

II. EXPERIMENT

The experimental setup (Fig. 1) has already been described elsewhere [4,5,11], but for coherence of the paper, it

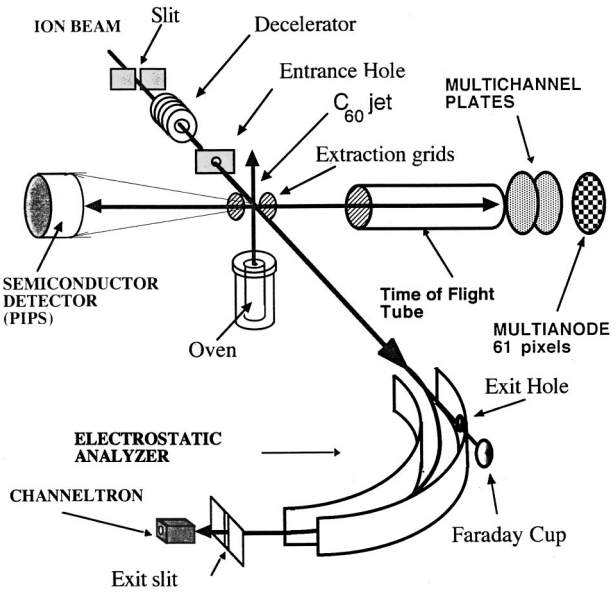

FIG. 1. Experimental setup.

is necessary to recall here a few features. The pressure in the collision chamber was maintained around 10^{-9} mbar during experiments to reduce the probability of collisions with the background gas composed mainly of CO, H_2 molecules. Multicharged ion beams were provided by the AIM facility in Grenoble. This device employed a 14 GHz ECR ion source from which Ar^{16+}, Kr^{16+}, and Xe^{16+} ion beams were extracted with 6, 11, and 17 kV voltages, respectively. These energies correspond to velocities of 0.28 a.u., taking into account a 1 kV deceleration before entering the interaction zone. Ion beams were collimated by a small entrance hole (500 μm) and measured with a pico-amperemeter connected to a Faraday cup situated behind another 500 μm exit hole (see Fig. 1). To ensure a good parallelism, the beams were driven in a way to optimize the ratio between the electric currents on the Faraday cup and on the external electrode of the cylindrical analyzer. The collision region, precisely aligned with both entrance and exit holes, was defined by the intersection at right angle between the ion beam and an effusive C_{60} gas jet produced by an oven heated at approximately 500 °C. Electrons and recoil ions were extracted towards opposite sides of the collision region by an electric field fixed to 1000 V/cm.

The measurement of σ_r^s cross sections is based on the determination, for each event, of the number s of stabilized electrons and of the number r of active electrons. The number s is easily obtained by selecting the final charge of the projectile by applying the appropriate symmetric voltages on both electrodes of the cylindrical analyzer. To determine the number r, one could collect and detect all charged fragments issued from the postcollisional fragmentation of the target, but this task is not trivial when the number of identical light fragments is too high. Our choice was to measure the number n of ejected electrons, in coincidence with the detection of a charge-selected projectile. The ejected electron number is determined by measuring the total energy deposited by all collected electrons in a semi-conductor detector (PIPS: Planar Implanted Passivated Silicon) after being accelerated by a 25 kV voltage. The number r is then obtained by summing up n and s according to the rule given above. Inversely, if we know exactly the numbers s and r for some particular events that can be selected by coincidence detection of a scattered projectile of charge $14+$ $(s=2)$ and a nonfragmented recoil C_{60}^{r+}, we can easily determine the number of ejected electrons $(n=r-s=r-2)$. The energy profile of the associated electron signal on the PIPS then allows us to determine the collection-detection efficiency of the ejected electrons. An example is given in Fig. 2 showing a biparametric spectrum [Fig. 2(a)] recorded for the incident projectile Ar^{16+}. In this spectrum, event counts are displayed as a function of the time of flight of recoil ions (X axis) and of the amplitude of the corresponding PIPS signal (Y axis) in coincidence with the scattered projectile Ar^{14+} $(s=2)$. The X projection of this spectrum [Fig. 2(b)] gives the usual time of flight spectrum associated with $s=2$. The main peaks correspond to nonfragmented multicharged fullerenes C_{60}^{3+},C_{60}^{4+}… The C_{60}^{+} and C_{60}^{2+} peaks (not shown in Fig. 2) that could result from double collisions are negligible. Partial Y projections of Fig. 2(a) were performed individually for each selected recoil ion peak C_{60}^{3+}, C_{60}^{4+}, C_{60}^{5+}, C_{60}^{6+} [Fig. 2(c)]. Each projection associated with a given C_{60}^{r+} peak presents a main peak at high energy corresponding to 25 keV times n $(=r-2)$, which is the expected number of ejected electrons

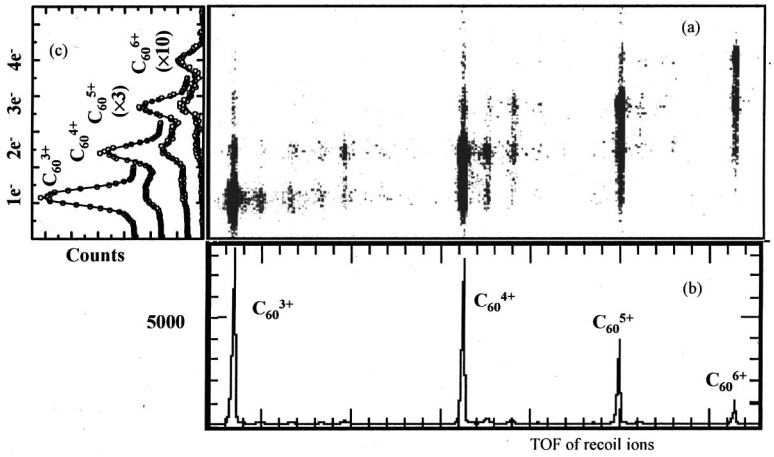

FIG. 2. (a) Ar^{16+}-C_{60}. 2D spectrum for triple coincidence between Ar^{14+} scattered ions ($s=2$), time of flight selected recoil ions, and electron signal. X axis represents the time of flight of recoil ions and Y is the amplitude of the PIPS signal, which is proportional to the total energy deposited by the electrons. (b) X projection of 2(a). (c) Partial Y projection of 2(b) for C_{60}^{3+}, C_{60}^{4+}, C_{60}^{6+}, and C_{60}^{7+}. Solid lines are fit curves (see text).

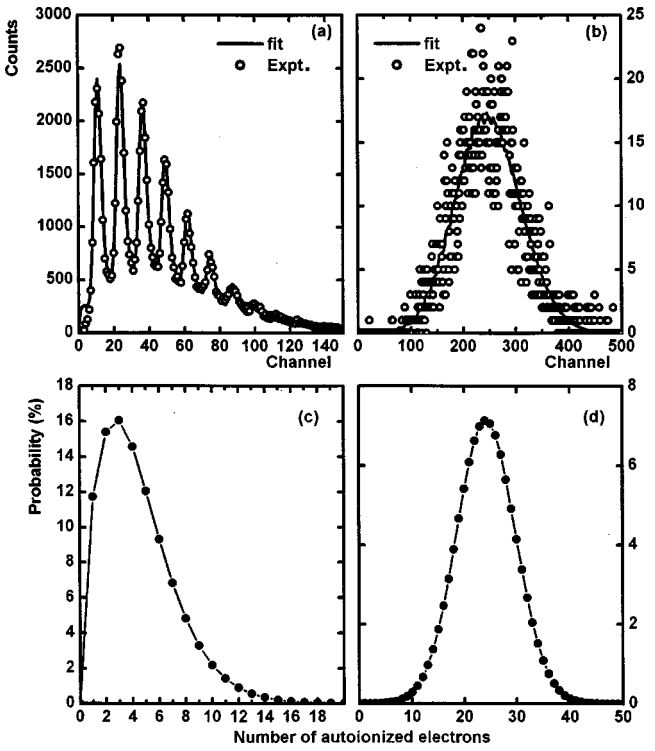

FIG. 3. Ar^{16+}-C_{60}. Electron spectra for (a) $s=2$ and (b) $s=7$ (c) and (d) represent the distributions of the number of autoionized electrons, i.e., n, that are employed to fit the experimental spectra in (a) and (c), respectively.

in the collision. On the low energy side, the distributions present secondary peaks that are due to backscattering of one (or several) electron from the Si solid and due to eventual electron losses. Each experimental electron energy distribution is fitted by a weighted sum of Gaussian functions following the results of Aumayr *et al.* [12]. The weighting factor contains the backscattering probability for 25 keV electrons in Si given in [12] ($\simeq$ 17%) and the collection probability for one electron which is adjusted to fit experimental data. Here collection probabilities were found to be about 0.9 for Ar^{16+}, Kr^{16+}, and Xe^{16+}. This value depends strongly on the electric field in the extraction region: the higher the field, the better the collection. It has been possible to roughly estimate the electron kinetic energy for the case Xe^{30+}-C_{60} by varying the extraction voltage, using the fact that the collection probability is related to the kinetic energy of the autoionized electrons [13]. This study has not been completed for the three collision systems in this paper but, since we observe approximately the same collection probability, we deduce that the energies of the autoionized electrons from the three projectiles are not too different.

The relative σ_r^s values were determined by recording coincidence counts between each outgoing projectile $A^{(q-s)+}$ and the electron signal amplitude while varying the analyzer voltage in order to integrate over the projectile energy gain (or loss) and the scattering angle. Figure 3 shows two representative electron spectra associated with $s=2$ [Fig. 3(a)] and $s=7$ [Fig. 3(b)] for Ar^{16+}-C_{60}. In Fig. 3(a), we observe well-separated peaks at energies corresponding to n times 25

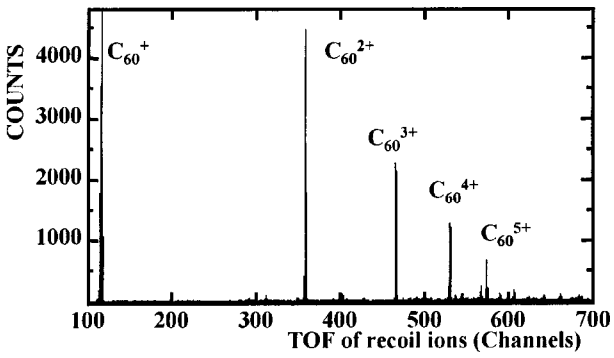

FIG. 4. Ar^{16+}-C_{60}. Time of flight spectrum associated with $s=1$ events. The relative amplitudes of the C_{60}^{+} and C_{60}^{2+} peaks were employed to determine the relative cross sections σ_1^1 and σ_2^1.

keV (with $n=1$, 2, 3 etc.). In the case of $s=7$ [Fig. 3(b)], the number of electrons to be detected at each event is so high that, due to the backscattering effect and the limited detection efficiency, no resolved peaks can be observed. By fitting the two experimental spectra taking into account both backscattering and detection efficiency effects, we determined the distributions of the number of autoionized electrons (n) for $s=3$ and $s=7$ [Figs. 3(c) and 3(d), respectively]. For $s=2$ the distribution is centered at $n=3$ or 4 [Fig. 3(c)] while for $s=7$ the center is obtained around $n=24$ [Fig. 3(d)]. Employing the same method, electron distributions are obtained for all other s values. The electron number distribution for each s value is in fact directly proportional to the cross section curve σ_r^s versus the number r of active electrons. To obtain the partial relative cross sections σ_r^s, a normalization to the total counts for different s values has been made taking into account the acquisition time and the beam intensity. However, this technique does not allow us to determine the relative cross section for processes without electron emission such as the single capture (σ_1^1) or the weaker stabilized double capture (σ_2^2) processes. Relative cross sections between σ_1^1 and autoionizing double capture (σ_2^1) are measured from the time of flight spectrum associated with $s=1$, as shown in Fig. 4 for Ar^{16+}-C_{60}. They are obtained by measuring the relative surfaces of the C_{60}^{1+} and C_{60}^{2+} peaks, after corrections due to different detection efficiencies of C_{60}^{+} and C_{60}^{2+} [6]. The same procedure is employed to determine the weaker σ_2^2 relative to σ_3^2 using the $s=2$ TOF spectrum. In order to give absolute cross sections σ_r^s (Fig. 5), the total cross section σ_t is normalized to a theoretical value estimated from an overbarrier calculation of the critical distance to capture one electron, R_a. We find $\sigma_t=\pi R_a^2=1.1\times10^{-13}$ cm^2 for projectiles of initial charge of 16+.

III. EXPERIMENTAL RESULTS

Figures 5(a), 5(b), and 5(c) show experimental partial cross sections σ_r^s for Ar^{16+}, Kr^{16+}, and Xe^{16+} colliding with C_{60}. Although logarithmic scales in Fig. 5 emphasize the less probable processes, collisions leading to $s=1$ or $s=2$ always dominate largely. Cross sections for $s>4$ are in gen-

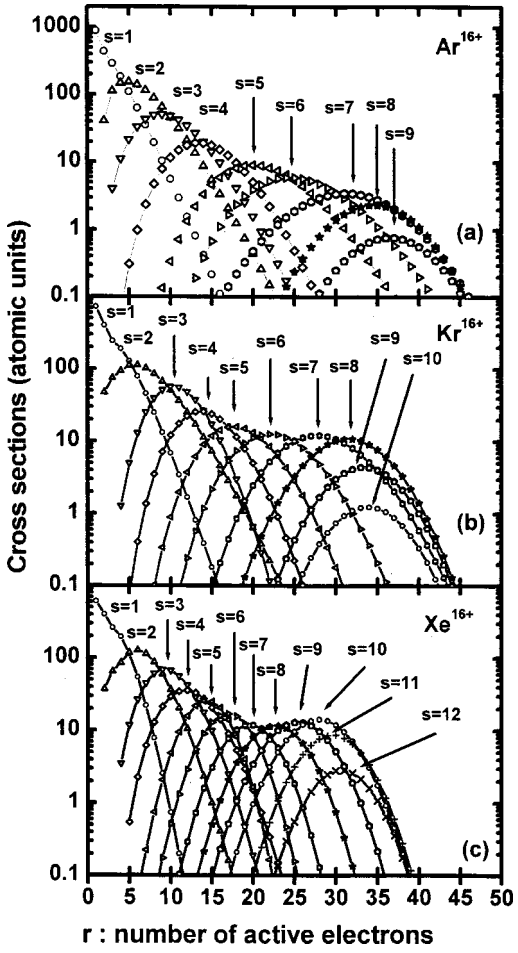

FIG. 5. Experimental partial cross sections σ_r^s for collisions of Ar^{16+} (top), Kr^{16+} (center), and Xe^{16+} (bottom) ions with C_{60}. Lines are to guide the eye.

eral at least two orders of magnitude smaller than for $s=1$. Nevertheless, our experimental technique allows us to measure cross sections up to $s_{max}=9$, 10, and 12 for Ar^{16+}, Kr^{16+}, and Xe^{16+}, respectively. No projectiles with a final charge lower than $(q-s_{max})$ could be significantly observed. In Fig. 5, we also note that the mean number of active electrons $\langle r\rangle$ for $s=s_{max}$ is about 37, 34, and 31 for Ar^{16+}, Kr^{16+}, and Xe^{16+}, respectively. As observed earlier with Xe^{30+}, the maximum number of active electrons can exceed two times the initial projectile charge. For each value of $s>2$, we remark that $\langle r\rangle$ is decreasing for increasing projectile atomic number; for instance, for $s=5$, $\langle r\rangle$ is 20, 17, and 14 for Ar^{16+}, Kr^{16+}, and Xe^{16+}, respectively. Conversely, for a given value of $\langle r\rangle$, lower s values are found for lighter projectiles. These two features emphasize the higher propensity of the Xe^{16+} to stabilize captured electrons than Kr^{16+} and Ar^{16+}. In the Xe^{16+} case, more electrons are stabilized for a given number of active electrons. In Fig. 6, $\langle r\rangle$ is plotted as a function of s, for s up to 9. For small values of r and s ($r\leqslant 10$ and $s\leqslant 3$) the three curves follow approximately the same trend showing that processes with few active electrons are mostly independent of the core structure of the projectile. Nevertheless, for each projectile, a linear curve fits correctly

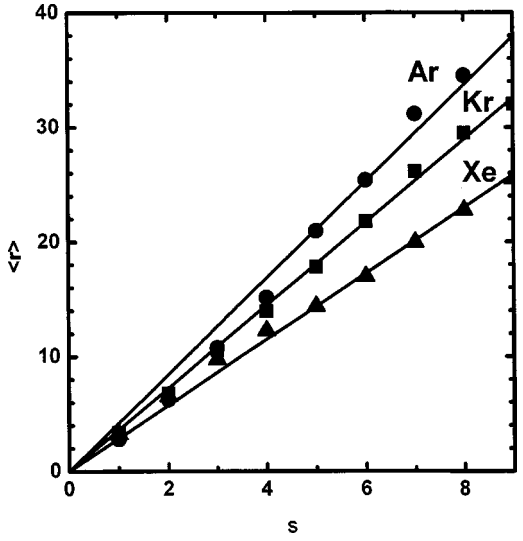

FIG. 6. Cross sections σ_r as a function of the number of active electrons (r) in collisions Ar^{16+}, Kr^{16+}, and Xe^{16+} (bottom) ions with C_{60}. For comparison, two classical overbarrier calculations are also shown with screening constant $\sigma=1$ (dashed line) and $\sigma=0$ (plain line).

the data points. Stabilization ratios reported in Table I (i.e., the number of active electrons per stabilized electron) are defined as the slopes of these fits. Figure 6 and Table I show that the lighter the projectile, the higher the stabilization ratio. Points for $s>9$ were not displayed in Fig. 6 because the main contribution in these cross sections is due to solidlike collisions for which the stabilization ratio follows a different law.

The cross sections for having r active electrons are obtained from the measured partial cross sections (Fig. 5) by the following relation: $\sigma_r=\Sigma_s\sigma_r^s$. In Fig. 7, σ_r is plotted as a function of r. For comparison, Fig. 7 displays also two curves corresponding to theoretical cross sections calculated from the overbarrier model taking into account a full screening and no screening of the initial charge of the projectile by previously captured electrons. The potential employed in our calculations was identical to the potential in Ref. [2] with inclusion of a screening parameter η:

$$V_R(x)=-\frac{q-(r-1)\eta}{|R-x|}+\frac{a[q-(r-1)]}{|Rx-a^2|}-\frac{a[q-(r-1)]}{|Rx|}-\frac{r}{|x|}+\frac{1}{2}\left(\frac{a}{x^2}-\frac{a}{|x^2-a^2|}\right). \quad (1)$$

TABLE I. Stabilization ratios ($\langle r\rangle/s$) for Ar^{16+}, Kr^{16+}, and Xe^{16+}. For indication, the sum of the 16 first ionization potentials V_{ion} of the three projectiles is given in column 2.

	$\langle r\rangle/s$	$\sum_1^{16} V_{ion}$ (keV)
Ar^{16+}	4.2	5.85
Kr^{16+}	3.6	3.65
Xe^{16+}	2.9	2.68

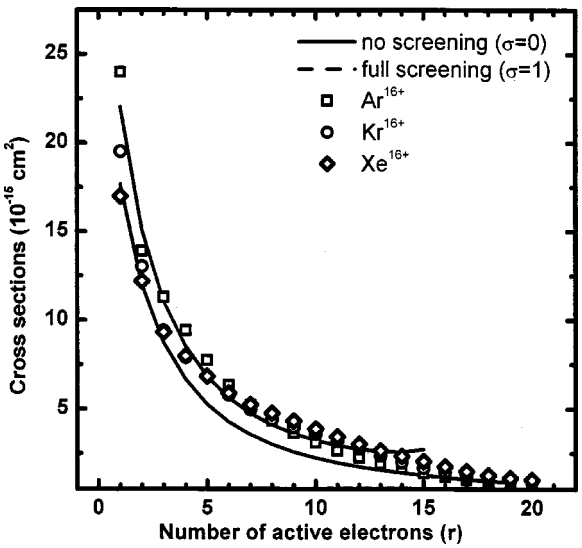

FIG. 7. Mean number of active electrons $\langle r \rangle$ as a function of the number of stabilized electrons (s) for collisions of Ar^{16+} (circles), Kr^{16+} (squares), and Xe^{16+} (triangles) ions with C_{60}. Lines are linear fits of each set of experimental data points.

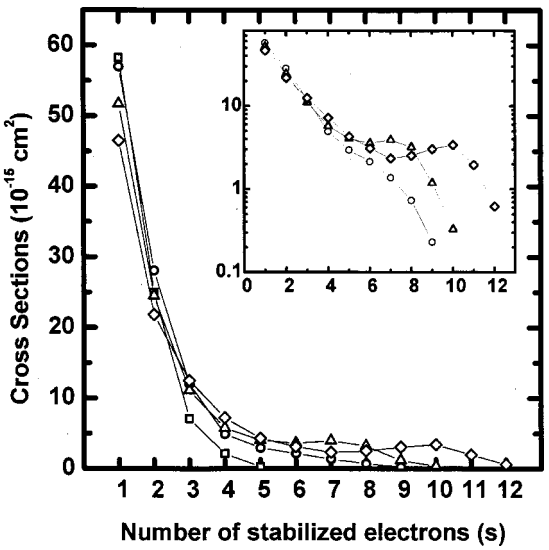

FIG. 8. Cross sections σ_s as a function of the number of stabilized electrons (s) for collisions Ar^{16+}, Kr^{16+}, and Xe^{16+} (bottom) ions with C_{60}. The inset represents the same curve but with a logarithmic scale on the Y axis in order to emphasize small cross sections at high s.

In Eq. (1), R and x are the distances of the projectile nucleus and of the rth active electron from the center of the C_{60}; q is the initial charge of the projectile and $a=8.2a_0$ (a_0 is the Bohr atomic radius) is the radius of the infinitely conducting sphere considered to describe the C_{60} given in Ref. [2]. The value of a is directly related to the polarizability α of the C_{60} by the relation $\alpha=a^3$. Antoine *et al.* [14] have performed a direct measurement of a and they found $\alpha=(517\pm54)a_0^3$, which gives $a=(8.0\pm0.3)a_0$. The determination of the theoretical cross sections σ_r (displayed in Fig. 7) follows then the classical method introduced in Refs. [2,8]. For the three projectiles, the tendency of experimental cross sections is well reproduced by the model either with $\eta=0$ or $\eta=1$. The full screening curves ($\eta=1$) are closer to the experimental cross sections for small r values but the number of captured electrons is theoretically limited to the initial projectile charge (here $q=16$), although for $\eta=0$, it is possible to consider the capture of the rth electron with $r>q$, as long as this electron still sees a positive charge on the projectile side.

The cross sections for producing (q-s) projectile final charge can also be deduced from Fig. 5 by summing over r: $\sigma_s=\Sigma_r\sigma_r^s$. The results are shown in Fig. 8 together with results from Langereis *et al.* [7] concerning Ar^{16+}-C_{60} collisions at a slightly lower velocity (0.23 a.u.). An overall good agreement is obtained between the two experiments, though the estimation of absolute cross sections was made differently, based on experimental data of C_{60} vapor pressure in Ref. [7] and on theoretical total cross section in our case. Nevertheless, we can remark a slight discrepancy in relative cross sections for the higher s values. It may be due to the difference in the projectile velocity or to a possible decrease in Ref. [7] of the collection efficiency of projectiles associated with high s values, which are known to have high scattering angles. In our experiment, the angle of acceptance of scattered projectiles is 2.3° though, in Ref. [7] where the authors refer to Ref. [15], the angle of acceptance is only 1°.

The inset in Fig. 8 represents the same data with a logarithmic scale in order to emphasize small cross section processes at high s. Although no clear dependence of σ_s on the projectile atomic core is observed until $s<5$, it appears that for higher s values the core effect is more evident. A small "hump" of the cross section appears for Kr^{16+} and for Xe^{16+}. This kind of behavior of σ_s has already been put in evidence for Ar^{8+} collisions and was attributed to solid-like collisions at very small impact parameters [1,4]. The absence of a hump for high s in the case of Ar^{16+} presents features similar to what we have reported [6] in the case of the bare O^{8+} collisions with C_{60}.

In previous papers, we have presented an experimental method, based on the measurement of the projectile energy loss, which allows us to separate the "IN" contribution due to solidlike collisions from the "OUT" contribution that groups atomlike and surfacelike regimes. Figure 9 shows IN and OUT σ_s cross sections as a function of s. The total IN cross sections are found to be 4.6, 6.9, and 7.2×10^{-15} cm^2 for Ar^{16+}, Xe^{16+}, and Kr^{16+}, respectively. They are in fairly good agreement with the geometrical surface of the C_{60}, which is 7.7×10^{-15} cm^2. For the IN contribution, we note that the distribution of the number of stabilized electrons s is centered at 6, 8, and 10 for Ar^{16+}, Kr^{16+}, and Xe^{16+}, respectively. Hence the final projectile charge ($q_f=16$-s) is centered at 10, 8, and 6 for the three projectiles, respectively. For interpretation, we follow the picture of Hattass *et al.* [16] of charge equilibration in SHCI—thin carbon foil collisions. In this model, it is assumed that in the solid, the charge of the projectile tends to q_e, the equilibrium charge estimated from the Bohr criterion $q_e=Z^{1/3}v$, where Z is the atomic number and v is the projectile velocity given in atomic units (here, $q_e\approx1$). An exponential decay from the initial charge to the equilibrium charge is employed to describe the evolution of the projectile charge as a function of the distance in the solid:

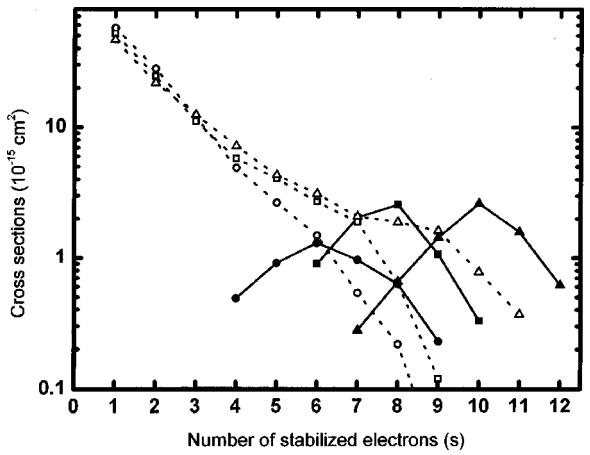

FIG. 9. Separated IN (dashed linkage and open symbols) and OUT (plain linkage and full symbols) contributions of σ_s for Ar^{16+} (circles), Kr^{16+} (squares), and Xe^{16+} (triangles). Straight linkage between points is to guide the eyes.

$$q = q_e + (q_i + q_e)\exp(-\alpha x/v). \tag{2}$$

In relation (2), α is the rate of charge equilibration and x is the effective thickness of the target. Given in s^{-1}, α is a phenomenological parameter depending on the nature of the projectile and the target. The parameter αx, which has the dimension of a velocity, is adjusted to fit our experimental data of Fig. 9. Results are shown in Table II. It can be admitted from what we know about capture models that for collisions with identical initial projectile charge, the effective width of the C_{60} target does not change significantly. Thus setting the C_{60} effective width to a reasonable value of 0.7 nm, we obtain the values for α that are listed in Table II. They are all in the order of magnitude of 10^{14} s^{-1}, which is comparable to values of Hattass *et al.* [16]. They found $\alpha = 4.7\times10^{14}$ s^{-1} for collision between Xe^{44+} ions and a carbon foil of 5 nm in width. These values of α indicate that charge equilibration is very fast so that many capture and autoionization processes can occur during the collision. Comparing the values of Table II, we observe that Xe and Kr ions have higher equilibration rates than Ar. Consequently, they tend faster to their equilibrium charge. Qualitatively, it is understood since Ar^{16+} ions offer more empty shells to fill before they reach their final exit charge.

IV. DISCUSSION

As shown in Fig. 7, the total cross sections σ_r depending on the capture processes are generally more or less independent of the initial electronic core of the projectile. This result is in agreement with the overbarrier model, which is basically only q dependant. Hence, in this section we mostly concentrate on projectile electron stabilization processes. In previous studies of double electron capture in SHCI–rare gas atom collisions, a strong projectile core dependence of the probability of stabilization of both electrons has been put in evidence [17]. In the hydrogenlike projectile case, the probability of radiative stabilization of both electrons on projectile has been measured to be three times lower than for bare ions. In contrast, the experimental results presented in the previous section show that core effects are rather small for the stabilization of a few electrons ($s \leqslant 3$). When the number of active electrons increases, the capture processes allow the population of lower levels of the projectile, stabilization of which is then more sensitive to the electronic structure of the atomic core. This feature is demonstrated by the stabilization ratios reported in Table I, which are found to be higher for lower atomic number projectiles. The sums of the 16 first ionization potentials are also given in Table I for Ar, Kr, and Xe. The correlation between a high stabilization ratio and a high total ionization potential is rather evident: the total ionization potential gives a good approximation of the total potential energy available for autoionizing electrons. Some attempts on using energy criteria in models consisting of distributing randomly the available energy on all captured electrons have been made. Such models are very promising for high active electron numbers and are expected to give the general trend of σ_r^s [18].

TABLE II. For IN collisions of Ar^{16+}, Kr^{16+}, Xe^{16+} with C_{60}, mean exit charge, αx parameter (dimension of a velocity), and charge equilibration time constant supposing $x = 0.7$ nm as an effective width for the C_{60}.

	Mean exit charge	αx (a.u.)	α (10^{14} s^{-1})
Ar^{16+}	10	0.14	4.4
Kr^{16+}	8	0.21	6.5
Xe^{16+}	6	0.26	8.2

In fact, the number of ejected electrons ($n = r - s$) is directly related to the number of transitions in the autoionizing cascade. For a given number of active electrons, assuming that the first steps of the cascade are identical for projectiles with identical initial charge, let us see how the transitions between the lowest levels will be affected by core effects. The electronic configurations of Ar^{16+}, Kr^{16+}, and Xe^{16+} are $1s^2$, $[Ar]3d^2$, and $[Kr]4d^2$, respectively. We assume, as an academic case, that after the previous autoionizing transitions, 8 of the captured electrons happen to be on the N shell of the projectile. In the Xe^{16+} case, the N shell being the lowest empty shell, we would have Xe^{8+} in its ground state so that no other autoionization process could occur. For Kr^{8+}, 8 holes remain in the M shell level, while for Ar^{8+} L and M shells are empty. If we only consider autoionization processes involving pairs of electrons, one of them being ejected into the continuum while the other one is transferred into the shell immediately below, Kr and Ar need then 4 and 6 transitions, respectively, to reach their fundamental state leading to 4 and 6 more ejected electrons than in the case of Xe. In Fig. 6, we observe for $\langle r \rangle = 20$ that Xe stabilizes 2 more electrons than Kr and 3 more than Ar. It means that, on average, 2 and 3 more electrons are ejected by Kr and Ar (respectively) than Xe. The above arguments overestimate the number of transitions in the final cascade. It should be due to the fact that the probability for the N shell to be occupied by 8 electrons at a given time is very low in the cases of Ar and Kr. To have a better understanding, a decay model following all possible steps of the cascade would be necessary. Unfortunately, so far, very few theoretical results

are available concerning autoionization decay rates of hollow atoms configurations. Nonetheless, recently, Palmeri *et al.* [10] have published calculations concerning a few configurations of hollow atoms. For instance, they find that the order of magnitude of the average lifetime is 10^{-16} s for hollow xenon with 20 excited electrons in the same $n=7$ or $n=10$ shells. In order to fulfill the goal of following the complete cascade more calculations are definitely needed.

V. CONCLUSION

We have measured partial cross sections for multicapture processes in collisions of Ar^{16+}, Kr^{16+}, and Xe^{16+} with C_{60}. We have observed that for atomlike collisions with few active electrons, the influence of the nature of the projectile (for a given charge) is rather small. This is explained by the fact that the lifetime of high Rydberg states populated in this case is weakly influenced by the core structure of the projectile. For collision processes with higher active electron number, population of lower shells is expected increasing thus the importance of the projectile core. Hence the stabilization ratio $(\langle r\rangle/s)$ has been found higher for Ar^{16+} than for Kr^{16+} and Xe^{16+}. Qualitative interpretation of this fact can be viewed in two ways; first, the number of empty shells and thus the number of steps in a cascade is higher for Ar^{16+}; secondly, in a statistical point of view, the available excitation energy to be redistributed among all active electrons is higher for Ar^{16+}. Despite recent calculations of hollow atom configurations, no complete treatment of the stabilization of these hollow atoms is presently available, since it seems an inextricable task to follow every possible step in a cascade and to evaluate the corresponding lifetimes. Another point of view to treat the problem of stabilization of hollow atoms would be to distribute in a statistical way the excitation energy among all active electrons and use an energy criterion to determine how many of them can be ejected to the continuum. We are rather confident in such a method to give good predictions for partial σ_r^s cross sections for the atomlike collision regime and results will be presented in a forthcoming paper. However, for surfacelike collisions, the situation is more problematic since one would have to treat simultaneously capture and stabilization processes.

ACKNOWLEDGMENTS

We are very grateful to H. Lebius and F. Gustavo for preparing high quality ion beams at the AIM facility in Grenoble. This work has been supported by the Region Rhône-Alpes under Grant Nos. 97027-223 and 97027-283, of the Convention Recherche, Program Emergence.

[1] B. Walch, L. C. Cocke, R. Voelpel, and E. Salzborn, Phys. Rev. Lett. **72**, 1439 (1994).
[2] H. Cederquist, A. Fardi, K. Haghighat, A. Langereis, H. T. Schmidt, S. H. Schwartz, J. C. Levin, I. A. Sellin, H. Lebius, B. Huber, M. O. Larsson, and P. Hvelplund, Phys. Rev. A **61**, 022712 (2000).
[3] J. Abrefah, D. R. Olander, M. Balooch, and W. J. Sieklaus (unpublished).
[4] S. Martin, J. Bernard, L. Chen, A. Denis, and J. Désesquelles, Eur. Phys. J. D **4**, 1 (1998).
[5] Jérôme Bernard, Li Chen, Alain Denis, Jean Désesquelles, and Serge Martin, Phys. Scr., **T73**, 286 (1997).
[6] L. Chen, J. Bernard, A. Denis, S. Martin, and J. Désesquelles, Phys. Scr., **T80**, 52 (1999).
[7] A. Langereis, J. Jensen, A. Fardi, K. Haghighat, T. D. Schmidt, S. H. Schwarz, H. Zettergren, and H. Cederquist, Phys. Rev. A **63**, 062725 (2001).
[8] U. Thumm, J. Phys. B **27**, 3515 (1994); **28**, 91 (1995).
[9] Serge Martin, Li Chen, Alain Denis, and Jean Désesquelles, Phys. Rev. A **59**, R1734 (1999).
[10] P. Palmeri, P. Quinet, N. Zitane, and N. Vaeck, J. Phys. B **34**, 4125 (2001).
[11] S. Martin, L. Chen, A. Denis, R. Brédy, J. Bernard, and J. Désesquelles, Phys. Rev. A **62**, 022707 (2000); S. Martin, L. Chen, A. Denis, J. Désesquelles, *ibid.* **57**, 4518 (1998).
[12] F. Aumayr, G. Lakits, and H. Winter, Appl. Surf. Sci. **47**, 139 (1991).
[13] R. Brédy, L. Chen, S. Martin, J. Bernard, and J. Désesquelles, Phys. Scr. (to be published).
[14] R. Antoine, Ph. Dugourd, D. Rayane, E. Benichou, M. Broyer, F. Chandezon, and C. Guet, J. Chem. Phys. **110**, 9771 (1999).
[15] S. H. Schwartz, A. Fardi, K. Haghighat, A. Langereis, H. T. Schmidt, and H. Cederquist, Phys. Rev. A **63**, 013201 (2000).
[16] M. Hattass, T. Schenkel, A. V. Hamza, A. V. Barnes, M. W. Newmann, J. W. McDonald, T. R. Niedermayr, G. A. Machicoane, and D. H. Schneider, Phys. Rev. Lett. **82**, 4795 (1999).
[17] S. Martin, J. Bernard, A. Denis, J. Désesquelles, and Li Chen, Phys. Rev. A **50**, 2322 (1994).
[18] Li Chen *et al.* (private communication).